Imaging Ca^{2+} Nanosparks in Heart With a New Targeted Biosensor

Wei Shang,* Fujian Lu,* Tao Sun, Jiejia Xu, Lin-Lin Li, Yanru Wang, Gang Wang, Liangyi Chen, Xianhua Wang, Mark B. Cannell, Shi-Qiang Wang, Heping Cheng

Rationale: **In cardiac dyads, junctional Ca^{2+} directly controls the gating of the ryanodine receptors (RyRs), and is itself dominated by RyR-mediated Ca^{2+} release from the sarcoplasmic reticulum. Existing probes do not report such local Ca^{2+} signals because of probe diffusion, so a junction-targeted Ca^{2+} sensor should reveal new information on cardiac excitation–contraction coupling and its modification in disease states.**

Objective: **To investigate Ca^{2+} signaling in the nanoscopic space of cardiac dyads by targeting a new sensitive Ca^{2+} biosensor (GCaMP6f) to the junctional space.**

Methods and Results: **By fusing GCaMP6f to the N terminus of triadin 1 or junctin, GCaMP6f-triadin 1/junctin was targeted to dyadic junctions, where it colocalized with t-tubules and RyRs after adenovirus-mediated gene transfer. This membrane protein-tagged biosensor displayed ≈4× faster kinetics than native GCaMP6f. Confocal imaging revealed junctional Ca^{2+} transients (Ca^{2+} nanosparks) that were ≈50× smaller in volume than conventional Ca^{2+} sparks (measured with diffusible indicators). The presence of the biosensor did not disrupt normal Ca^{2+} signaling. Because no indicator diffusion occurred, the amplitude and timing of release measurements were improved, despite the small recording volume. We could also visualize coactivation of subclusters of RyRs within a single junctional region, as well as quarky Ca^{2+} release events.**

Conclusions: **This new, targeted biosensor allows selective visualization and measurement of nanodomain Ca^{2+} dynamics in intact cells and can be used to give mechanistic insights into dyad RyR operation in health and in disease states such as when RyRs become orphaned. (*Circ Res*. 2014;114:412-420.)**

Key Words: biosensing techniques ■ calcium signaling ■ excitation-contraction coupling ■ junctin ■ ryanodine receptor calcium release channel ■ triadin

Cardiac contraction is caused by intracellular Ca^{2+} release as a result of signaling in a nanoscopic domain, the dyad, formed from the close apposition of the sarcoplasmic reticulum (SR) and surface membranes.[1] Two types of Ca^{2+} channels, the voltage-gated L-type Ca^{2+} channels, which control Ca^{2+} influx elicited by action potentials, and ryanodine receptors (RyRs), which mediate Ca^{2+} release from intracellular stores, reside on the surface and SR membranes of the dyad, respectively. Orthograde L-type Ca^{2+} channel-to-RyR coupling is mediated by the Ca^{2+}-induced Ca^{2+} release mechanism, whereas retrograde coupling controls the L-type Ca^{2+} channel current within the same beat.[2]

In This Issue, see p 395
Editorial, see p 396

Whole-cell Ca^{2+} transients during cardiac excitation–contraction (EC) coupling were first seen as aequorin bioluminescence in frog cardiac muscle[3] and in canine Purkinje fibers.[4] The creation of small-molecule chemical fluorescence indicators, such as fura-2,[5] catalyzed an explosion of Ca^{2+} imaging activity in single cardiac myocytes under normal conditions[6] and during Ca^{2+} overload when propagating waves of elevated Ca^{2+} were observed.[7] With the advent of confocal microscopy and the fast, high-contrast Ca^{2+} indicator fluo-3, the discovery of Ca^{2+} sparks,[8] which is the result of single-dyad Ca^{2+} signaling, has revolutionized our understanding of cardiac EC coupling and the spatiotemporal summation of ≈10^4 elemental Ca^{2+} sparks results in a global Ca^{2+} transient that controls cell contraction. From the viewpoint of control theory, such digital behavior is quintessential for enabling high-speed, high-gain amplification with

Original received October 29, 2013; revision received November 19, 2013; accepted November 20, 2013. In October 2013, the average time from submission to first decision for all original research papers submitted to *Circulation Research* was 12.81 days.

From the State Key Laboratory of Biomembrane and Membrane Biotechnology, Beijing Key Laboratory of Cardiometabolic Molecular Medicine, Institute of Molecular Medicine, Peking-Tsinghua Center for Life Sciences (W.S., F.L., T.S., J.X., Y.W., G.W., L.C., X.W., H.C.) and State Key Laboratory of Biomembrane and Membrane Biotechnology, College of Life Science (L.-L.L., S.-Q.W.), Peking University, Beijing, China; and Department of Physiology and Pharmacology, University of Bristol, City of Bristol, United Kingdom (M.B.C.).

*These authors contributed equally to this article.

The online-only Data Supplement is available with this article at http://circres.ahajournals.org/lookup/suppl/doi:10.1161/CIRCRESAHA.114.302938/-/DC1.

Correspondence to Heping Cheng, PhD, Institute of Molecular Medicine, Peking University, Beijing 100871, China (e-mail chengp@pku.edu.cn); or Shi-Qiang, PhD, Wang, College of Life Science, Peking University, Beijing 100871, China (e-mail wsq@pku.edu.cn).

Nonstandard Abbreviations and Acronyms	
EC coupling	excitation–contraction coupling
F/F_0	normalized fluorescence where F_0 refers to the resting fluorescence
$(F/F_0)_d$	F/F_0 deconvolved with a single-exponential kernel reflecting turn-off rate of the biosensor
GCaMP6f-T	GCaMP6f fused to triadin 1
GCaMP6f-J	GCaMP6f fused to junctin
RyR	ryanodine receptor
SR	sarcoplasmic reticulum

stability in EC coupling.[9,10] The process of cardiac EC coupling is therefore a tale of signaling in cellular nanodomains whose regulation remains a focus of intense research worldwide.

However, fluorescent Ca^{2+} imaging techniques with diffusible indicators (eg, see ref. 11) do not reveal either the underlying Ca^{2+} signaling process or the behavior of the RyRs at the level of the dyad without considerable computational difficulty and uncertainties (eg, see ref. 11). Furthermore, Ca^{2+} sparks are not easily detected once whole-cell release starts and $\approx 10^4$ dyads are activated near synchronously. The measurement of Ca^{2+} spikes[12] provided a way to overcome this problem, but it requires the inclusion of high concentrations of an exogenous, slow Ca^{2+} buffer (eg, EGTA), which will disturb the Ca^{2+}-induced Ca^{2+} release process as well as other signaling processes that depend on Ca^{2+}. A new method to probe dyadic space dynamics directly could therefore give insightful information into how RyRs are regulated, as well as check the veracity of new models for RyR array operation and release termination.[13,14]

The dyadic space is $\approx 10^{-3}$ fl (1 al),[15] a volume that would preclude obtaining useful dyadic Ca^{2+} signals using conventional fluorescent probes. Here, we describe a new approach to this problem using a targeted high-sensitivity biosensor construct for Ca^{2+}-GCaMP6f.[16] By attaching GCaMP6f to the dyad junctional proteins junctin or triadin,[17] we show that high signal-to-noise records of Ca^{2+} changes in the dyad, which we call Ca^{2+} nanosparks, can be obtained without complications from indicator diffusion. Ca^{2+} nanosparks are $\approx 50\times$ smaller in volume than Ca^{2+} sparks and can display substructure and gradation at the single dyad level. We also present exemplar data from adult rat cardiac myocytes showing evoked Ca^{2+} signals at single dyads, which should afford a new way of investigating spatiotemporal synchrony (or dyssynchrony) in EC coupling in heath and disease.

Methods

Adult Rat Cardiac Myocytes Isolation, Culture, and Adenovirus Infection

Animals were treated in compliance with the Guide for the Care and Use of Laboratory animals published by the US National Institutes of Health (Publication No.85-23, revised 1996) and approved by the Institutional Animal Care and Use Committee of Peking University (accredited by Association for Assessment and Accreditation of Laboratory Animal Care international). Single ventricular myocytes were enzymatically isolated from the hearts of adult male Sprague–Dawley rats (200–250 g), as described previously.[18] Freshly isolated cardiac myocytes were plated on culture dishes coated with laminin (Sigma) for 1 hour and then the attached cells were cultured in M199 medium (Sigma) added with (in mmol/L) 5 creatine, 2 L-carnitine, 5 taurine, 25 HEPES (all from Sigma), and insulin-transferrin-selenium-X (Gibco). Cardiac myocytes were then infected with adenovirus carrying the target gene at an multiplicity of infection of 20 and experiments were performed after 48 hours in culture.

Recombinant Adenovirus Production

The *GCaMP6f* gene was amplified from pGP-CMV-GCaMP6f (Addgene, plasmid 40755) and inserted into pEGFP-C1 (Clontech). The rat *triadin 1* and *junctin* genes were cloned and integrated into pEGFP-C1-GCaMP6f with *GCaMP6f* at the N terminus. The fusion genes *GCaMP6f-triadin 1* (*GCaMP6f-T*) and *GCaMP6f-junctin* (*GCaMP6f-J*) were then amplified and inserted into pENTR/TEV/D-TOPO vector (Invitrogen). The adenovirus was produced using the Invitrogen adenoviral expression system (Invitrogen).

Immunofluorescence Assay

Cardiac myocytes were permeabilized with 0.5% Triton X-100 and blocked with 10% normal goat serum. The sections were incubated with anti–RyR monoclonal antibody (Sigma, R128) for 2 hours at room temperature, washed with PBS, and then incubated with tetrarhodamine isothiocyanate–conjugated goat anti-rabbit IgG (Santa Cruz) for 1 hour at room temperature. The immunofluorescence staining was visualized using Zeiss LSM710 confocal microscope at 488 nm (GCaMP6f-T/J) and 543 nm (tetrarhodamine isothiocyanate) excitation and 490 to 550 nm and >560 nm emission, respectively.

Unmixing of Di-4 AN (F) PPTEA and GCaMP6f-J Signals

Di-4 AN (F) PPTEA (Di-4, 0.5 μg/mL, 5 minutes), a lipophilic dye,[19] was used to stain the surface membrane and t-tubules in cultured cardiac myocytes expressing GCaMP6f-J. With excitation at 488 nm, spectral images covering 486 to 719 nm were collected with an inverted confocal microscope (Zeiss NLO710) equipped with a 34-Channel QUASAR Detection Unit. For unmixing the Di-4 and GCaMP6f-J components, the reference spectra were obtained in Di-4–stained, uninfected cells and GCaMP6f-J–expressing, Di-4–unstained cells, respectively.

In Situ Calibration of the Biosensor

Adult rat cardiac myocytes expressing GCaMP6f-T/J were permeabilized with 50 μg/mL saponin and then treated with internal solution containing (in mmol/L) 10 KOH, 100 aspartic acid, 20 KCl, 0.81 $MgCl_2$, 3 Mg-ATP, 0.5 EGTA, 5 phosphocreatine ditris, 10 phosphocreatine-Na, 5 creatine phosphokinase, 10 glutathione, 8% dextran, and 20 HEPES and different concentrations of Ca^{2+} (from 3×10^{-9} to 2×10^{-5} mol/L at pH 7.2). The fluorescence of GCaMP6f-T/J was recorded with Zeiss LSM710 confocal microscope with 488 nm excitation and 490 to 550 nm emission as was also used for fluo-4 measurement. The relationship of Ca^{2+} concentration (C) and normalized fluorescence (R) or $(F-F_{min})/(F_{max}-F_{min})$, where F_{min} (minimum biosensor fluorescence) and F_{max} (maximal fluorescence of the biosensor) were obtained at 3×10^{-9} and 2×10^{-5} mol/L, respectively, was fitted with the equation $R=C^{nH}/(K_d^{nH}+C^{nH})$, where nH is the Hill coefficient and K_d is the dissociation constant.

Confocal Imaging

Confocal imaging was performed with a Zeiss LSM710 microscope with a 63×, 1.4 NA oil immersion objective, and linescan speed of 1.53 ms/line, the pinhole was set for a nominal 1 μm optical section. For simultaneous measurement of GCaMP6f-T/J and Rhod-2, excitation was at 488 and 543 nm and their fluorescence emission was collected at 490 to 550 and >560 nm, respectively. For chemical Ca^{2+} indicator loading, cultured cardiac myocytes were incubated with 5 μmol/L rhod-2 AM (Invitrogen) or fluo-4 AM (Invitrogen) for 10 minutes at room temperature.

Image Processing and Data Analysis

Digital images were processed using customer-devised routines written in Interactive Data Language (ITT, New York, NY). To obtain the time course of fluorescence corrected for the biosensor's turn-off

kinetics, deconvolution was performed with Wiener filter in the frequency domain. The degenerate kernel used in the Wiener filter was a single-exponential decay function with time constant of 60 ms reflecting the turn-off rate of the biosensor.

Statistics

Data are reported as the mean±SE. Student *t* test and the Mann–Whitney *U* test for nonparametric distributions were applied, when appropriate, to determine the statistical significance of differences. $P<0.05$ was considered statistically significant.

Results

Targeting the Ca^{2+} Biosensor GCaMP6f to Junctional SR

The rationale for developing a sensitive (instead of low affinity)-targeted Ca^{2+} biosensor is to probe dyad junctional Ca^{2+} dynamics, which has not been possible with cytoplasmic probes. We reasoned that a genetically encoded Ca^{2+} probe linked to known junctional proteins (triadin1 and junctin) should concentrate the biosensor into the high Ca^{2+} nanodomain associated with RyR activity (Figure 1A). This approach should avoid the potential complication arising from tagging RyRs themselves which might alter their gating and/or assembly in the dyad. As to the biosensor of choice, the latest generation of fluorescent protein–based Ca^{2+} probe GCaMP6f seems to be ideal because of its fast kinetics (the fastest among all currently known GCaMPs), high affinity (relative to junctional calcium), and superb contrast factor.[16] In a recent study, it was successfully implemented in measuring single synapse events,[16] leading to an important breakthrough in understanding dendritic integration.

In cultured rat ventricular myocytes 48 hours after adenoviral-mediated gene transfer, confocal imaging revealed that GCaMP6f-T and GCaMP6f-J (triadin 1 and junctin constructs, respectively) were enriched at punctate sites forming striated sarcomeric pattern (Figure 1B and 1C). This result suggests that both triadin 1 and junctin can target correctly their N-terminal–fused GCaMP6f to the dyadic clefts. This notion was confirmed by colocalization of GCaMP6f-J and GCaMP6f-T (latter data not shown) with type 2 RyR immunofluorescence (Figure 1C) and the pattern of labeling was similar to that reported in high-resolution studies of RyR distribution.[20] The t-tubular structure of the myocytes was well maintained with GCaMP6f-J and Di-4 fluorescent signals (a surface membrane marker) strongly colocalizing (Figure 1D) after spectral unmixing (Online Figure I) again supporting the idea that the construct correctly trafficked to the dyadic junctions.

GCaMPs are circularly permuted variants of enhanced green fluorescent protein coupled to the Ca^{2+}-binding protein

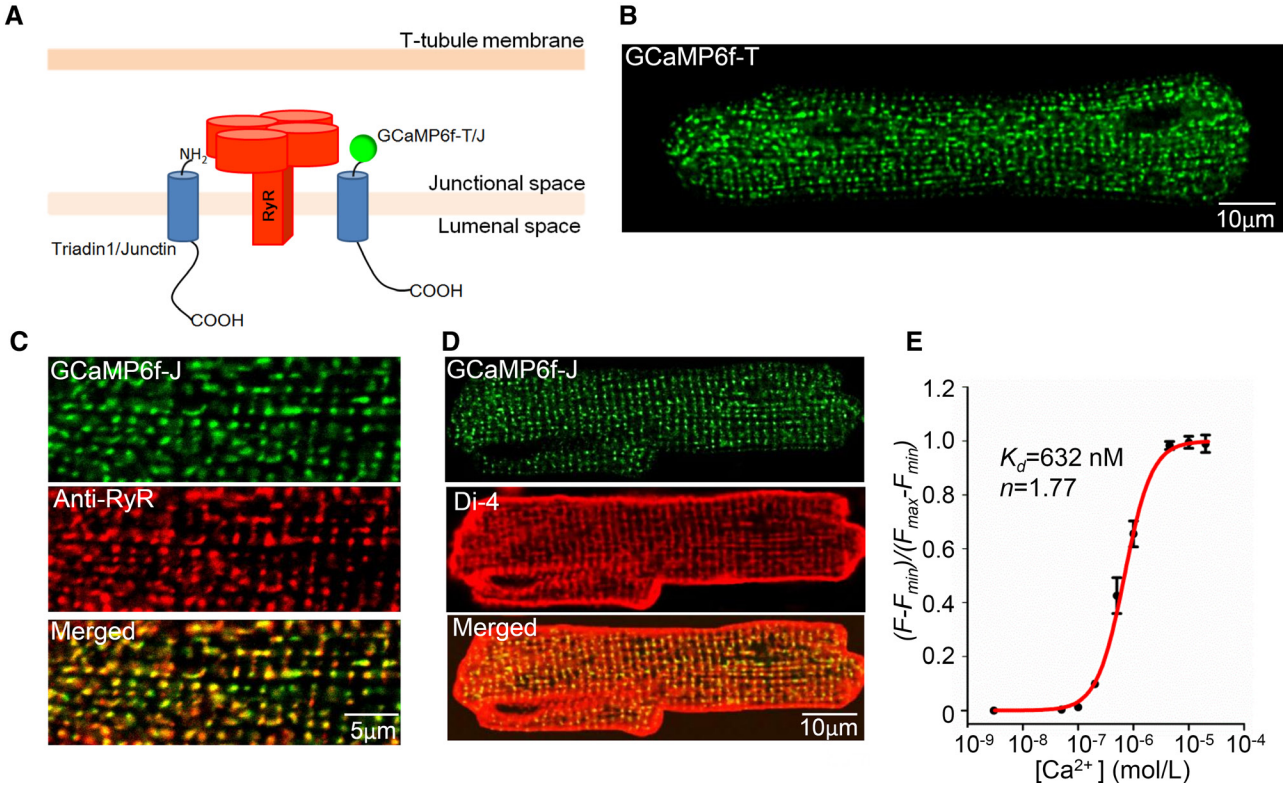

Figure 1. Targeting the Ca^{2+} biosensor to dyadic clefts. A, Targeting strategies. GCaMP6f was fused to the N terminus of the dyadic proteins triadin 1 (GCaMP6f-T) or junctin (GCaMP6f-J) and was expressed in cultured adult rat ventricular myocytes by adenoviral infection. **B**, Intracellular localization of GCaMP6f-T. Note the punctate appearance of the fluorescence. **C** (**top** to **bottom**), GCaMP6f-J fluorescence, RyR2 immunolabeling, and colocalization of GCaMP6f-J and RyR2. Similar results were found with GCaMP6f-T. **D** (**top** to **bottom**), GCaMP6f-J fluorescence, the surface membrane marker Di-4 and merged image. Note the preservation of radial t-tubule structure and that the punctate GCaMP6f-J fluorescence occurs along the t-tubules. **E**, In situ calibration. Saponin-permeabilized, biosensor-expressing cardiac myocytes were exposed to a solution containing the indicated free Ca^{2+}. Minimal (F_{min}) and maximal (F_{max}) fluorescence of the biosensor were measured at 3 nmol/L and 20 μmol/L Ca^{2+}, respectively. The solid curve is a Hill equation fit to the data with parameters as indicated.

calmodulin at the C terminus as the Ca^{2+} sensor, and a calmodulin-binding M13 peptide at the N terminus.[21] Crystal structures of GCaMP2 have shown that, on Ca^{2+} binding, the calmodulin moiety interacts and interlocks with the M13 peptide, causing a significant structural reorganization in proximity to the chromophore of cpEGFP and increasing its fluorescence, probably by deprotonating the chromophore.[22] To assess the performance of the dyad-targeted GCaMP6f-T/J, we measured fluorescence changes in saponin-permeabilized cells when bathing Ca^{2+} was increased from 3 nmol/L to 20 μmol/L. GCaMP6f-T/J in cardiac dyads displayed a contrast factor of 42.5±11 (n=6 cells) defined as the ratio of F_{max} to F_{min}, similar to that observed in vitro.[16] Nonlinear fitting yielded a K_d of 632 nmol/L and a Hill coefficient (n) of 1.77 (Figure 1E). Interestingly, GCaMP6f-T/J displayed an off rate ≈4-fold faster than that of native GCaMP6f (see below). Thus, we have succeeded in creating a novel Ca^{2+} biosensor that colocalizes with t-tubules and RyRs at dyadic clefts, offering a new approach to detecting nanodomain Ca^{2+} changes.

Imaging Dyadic Ca^{2+} Nanosparks With GCaMP6f-T/J

Spatially discrete, sudden, and transient GCaMP6f-T/J fluorescence increases (Ca^{2+} nanosparks; see Discussion) arose spontaneously from biosensor-labeled dyads in resting cardiac myocytes (Figure 2A and 2B). Nanosparks rose abruptly, attained a peak of 3.0 (F/F_0) in ≈22 ms, and then returned to the baseline with single-exponential kinetics (time constant of the decay of biosensor fluorescence [τ_{decay}]≈63 ms; Figure 2; Table). Individual nanosparks were confined to focal regions of the cell (width≈540 nm; Table), with no evidence of a diffusive fluorescence signal affecting ambient space (or neighboring sites). Given the limited confocal resolution, the size of these regions seems consistent with recent tomographic data on dyadic junctions.[23] When compared with Ca^{2+} sparks

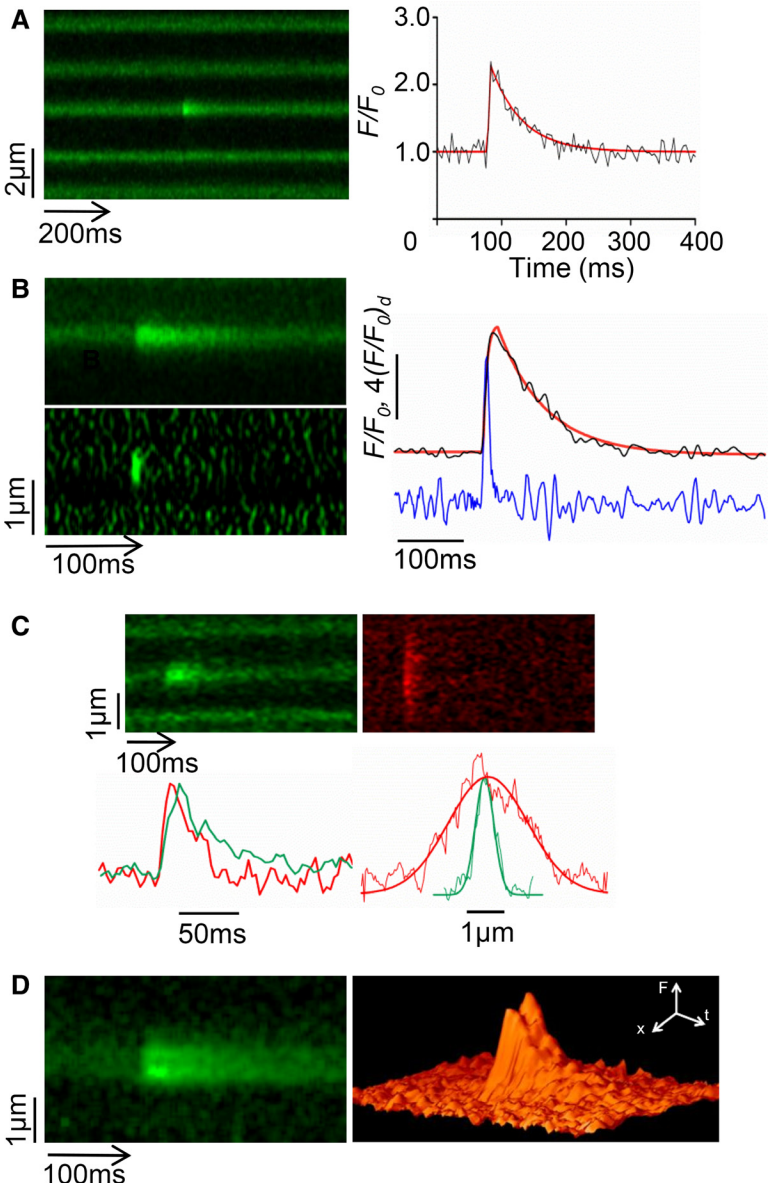

Figure 2. Ca^{2+} nanosparks probed with GCaMP6f-triadin 1/junctin (GCaMP6f-T/J). A, **Left**, Linescan image of a Ca^{2+} nanospark detected with GCaMP6f-T. **Right**, Time course of fluorescence change and an exponential fit to the rise and the decay (solid line). **B**, Exemplar Ca^{2+} nanospark detected with GCaMP6f-J. **Left**, Linescan image before (**top**) and after deconvolution using a single-exponential kernel (**bottom**) reflecting a biosensor's dissociation rate constant (K_{OFF}) ≈17/s. **Right**, Original (upper trace, F/F_0) and deconvolved time course (lower trace, $(F/F_0)_d$) of the nanospark. **C**, **Top**, A typical Ca^{2+} nanospark (**left**) with a simultaneously recorded Ca^{2+} spark using rhod-2 (**right**). **Bottom**, Time course and spatial extent of both event signals. Note the slower decay time but decreased spatial extent of the Ca^{2+} nanospark (green) compared with the Ca^{2+} spark (red). **D**, Example of substructure present in some Ca^{2+} nanosparks. The surface plot at the **right** shows the space–time evolution of the intrajunctional signal.

Table. Comparison of Ca^{2+} Spark and Nanospark Properties

Calcium Indicator	F/F_0	Time to Peak, ms	T50, ms	τ, ms	FDHM, ms	FWHM, nm	n
GCaMP6f-T/J	2.93±0.13	22.5±1.38	36.3±1.97	65.0±3.00	53.2±2.30	542±15.9	48
GCaMP6f-T/J(rhod-2)	3.18±0.17	21.5±1.29	37.9±1.71	61.7±2.78	53.7±2.17	547±17.0	41
rhod-2(GCaMP6f-T/J)	1.77±0.11	21.3±1.55	33.5±4.49	...	49.7±4.80	2196±129	19
rhod-2	1.58±0.05	21.1±1.77	33.6±2.18	...	48.8±2.49	2068±94.4	37
fluo-4	2.03±0.09	16.1±0.87	30.7±2.58	...	42.2±2.90	2197±93.0	52

Data are presented as mean±SEM. No significant differences between rhod-2 sparks in biosensor-free vs GCaMP6f-T/J-expressing cells. GCaMP6f-T/J indicates GCaMP6f-triadin 1/junctin; FDHM, full duration at half maximum; FWHM, full width at half maximum; and T50, time for 50% decay from peak.

reported by rhod-2 (Figure 2C), Ca^{2+} nanosparks occupied a 50× smaller optical volume but were significantly brighter (Table). Ca^{2+} nanosparks were completely abolished by SR-Ca^{2+} depletion with 20 mmol/L caffeine but persisted in the presence of the L-type Ca^{2+} channel inhibitor nifedipine (10 μmol/L; data not shown). Hence, these GCaMP6f-T/J fluorescent nanosparks reflect the first direct visualization of Ca^{2+} signals in the dyad junctional space.

The immobility of GCaMP6f-T/J implies that Ca^{2+} nanospark formation is simply driven by the local Ca^{2+} turning ON the biosensor, convolved with the biosensor's OFF kinetics. Specifically, the ON process reflects the rise of local Ca^{2+}, the Ca^{2+} binding to the calmodulin moiety of the biosensor, and the deprotonating rearrangement around the chromophore before fluorescence emission, whereas the OFF process (dissociation rate constant [K_{OFF}]) reflects the deactivation of the chromophore. After RyR closure, local Ca^{2+} gradients collapse rapidly[24,25] so that the onset of nanospark decline should give a measure of the time taken for complete RyR closure, and the decline rate of nanosparks should be mainly determined by the OFF kinetics of the biosensor. Furthermore, the time course and amplitude (F/F_0) of nanosparks should not depend on relative position of the dyad to the confocal plane, providing that contaminating background fluorescence from other sources is negligible (see below).

As shown in the Table, the time to peak of nanosparks was longer than the typical time to peak of a Ca^{2+} spark.[8] The histogram of τ_{decay} exhibited a major Gaussian component that centered around 60 ms, with a small tail reflecting a subpopulation of prolonged release events (Online Figure II). These data suggest that the turn-off rate of the targeted biosensor in situ was ≈17/s, a ≈4-fold improvement compared with its tag-free counterpart.[16] Importantly, by simultaneously measuring rhod-2 Ca^{2+} signals, we found that the presence of the biosensors did not significantly alter the time course or amplitude of spontaneous Ca^{2+} sparks (Table). This result indicates that biosensor expression exerted negligible buffering effects on the evolution of dyadic Ca^{2+} that controls EC coupling.

Based on the nanospark formation mechanism described above, the time course measurement can be improved by temporal deconvolution using a kernel reflecting the turn-off kinetics of the biosensor. Using K_{OFF}=17/s to approximate the OFF kinetics of the biosensor, we deconvolved the nanospark and used the resulting trace, $(F/F_0)_d$, as a more direct indicator of junctional Ca^{2+} dynamics (Figure 2B). A representative linescan image of kinetically deconvolved Ca^{2+} nanospark $(F/F_0)_d$ and its corresponding spatially averaged line plot are shown in Figure 2B. On average, $(F/F_0)_d$ reached its peak at ≈12 ms from onset, in reasonable agreement with detailed modeling and release flux calculations for rat with the release flux reaching a peak at ≈5 ms and lasting for ≈20 ms.[24,26]

RyR Array Operation at Single Dyads

With the precise colocalization of the biosensor and the Ca^{2+} source, the superior dyad-to-background contrast, and the high sensitivity provided by targeted GCaMP6f-T/J, we investigated RyR array operation at the single-dyad level. Although Ca^{2+} nanosparks generally appeared as a single homogeneous region, in some cases distinct substructure could be resolved. Figure 2D illustrates such an event with the fluorescence increase occurring in 2 linked regions nearly simultaneously (as far as can be determined from the limited time resolution of the microscope and signal-to-noise ratio). We suggest that such events reflect the activation of separate RyR clusters within the same junctional space, which coactivate in <4 ms. Furthermore, we found that the Ca^{2+} nanospark amplitude, measured at the origin of Ca^{2+} release and relatively immune to out-of-focus blurring, displayed a broad distribution (Online Figure IIIA), ranging from 1. 8 to 4.8 (F/F_0 at 5 and 95 percentiles) with a mean value of 3.04. Similarly, after temporal deblurring, peak $(F/F_0)_d$ varied from 4.1 (at 5%) to 14.9 (at 95%; Online Figure IIIB). Taken together, these data provide novel evidence for the possibility of stochastic recruitment of different numbers of RyRs within Ca^{2+} nanosparks.

We also examined dyads displaying >1 Ca^{2+} nanospark. Figure 3A and 3B illustrates variability in peak F/F_0 and $(F/F_0)_d$ in consecutive Ca^{2+} nanosparks. The smallest Ca^{2+} nanosparks are similar to single-quanta[13] and quarky Ca^{2+} release events as reported previously.[27] For pairs of Ca^{2+} nanosparks at the same dyads, their peak F/F_0 ranged from 0.75 to 1.33 (at 5 and 95 percentiles, respectively) with peak $(F/F_0)_d$ from 0.48 to 2.2 (Figure 3C). Thus, the gradation of amplitude reflects an event-to-event stochastic recruitment of individual or subclustered RyRs.

Imaging Dyadic Activation During EC Coupling

Next, we examined junctional Ca^{2+} dynamics during normal (ie, electrically evoked) EC coupling. Representative results in Figure 4 illustrate several novel features. First, in cardiac myocytes undergoing electric pacing, the Ca^{2+} transients occurred in discrete domains that did not merge (unlike other Ca^{2+} reporter signals). Because of this, timing of activation at individual dyads was clearly resolved in vigorously contracting cells. Second, dyads displaying 2-fold difference in F_0, perhaps reflecting in-focus and slightly out-of-focus sites had similar F/F_0 (Figure 4B and

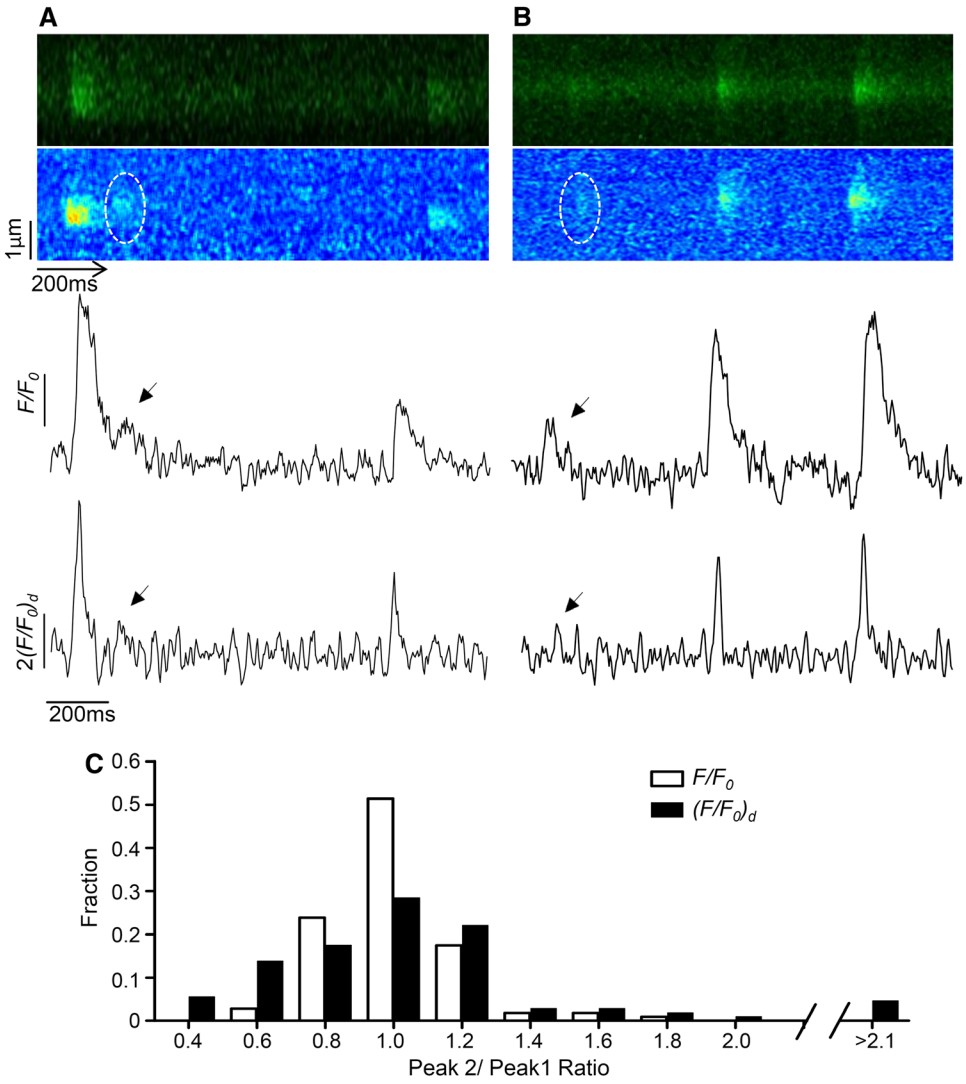

Figure 3. Ca^{2+} release at single dyads. A, Ca^{2+} nanosparks of variable amplitudes. **Top** to **bottom**, raw (**top**) and normalized (F/F_0) linescan images, time course of the nanosparks, and their corresponding deconvolved trace $(F/F_0)_d$. The dashed circle in the F/F_0 image and the arrow in the line plots indicate a quarky Ca^{2+} release event in the decline phase of the first nanospark. **B**, Another example as in **A**. Note the changing strength of the consecutive Ca^{2+} nanosparks at the same dyad. **C**, Histogram showing single-dyad variability of Ca^{2+} nanospark amplitudes. A total of 109 pairs of nanosparks at the same dyads were obtained and their pair-wise ratios of the nanospark amplitude (F/F_0, blank bars; $(F/F_0)_d$, filled bars) are plotted.

4C). This is because of the probe being fixed so that the relative change in fluorescence is unaffected by the sensitivity of the optical detector (in this case being determined by the limited extent of the microscope point spread function). Third, at dyads that were activated late, we observed a slow transient preceding a sudden, rapid upstroke of the dyadic signal. We interpret the first phase to result from cytosolic Ca^{2+} transient that invades the junctional space, and the second phase to reflect evoked dyadic release in the form of a Ca^{2+} nanospark. Remarkably, the properties of these late Ca^{2+} nanosparks were similar to those of early ones, directly showing (for the first time) that inferred SR depletion in adjacent sites during EC coupling[28] has minor effects on the proximal SR store on the time scale of normal Ca^{2+} release. Furthermore, the fully activated dyadic Ca^{2+} signal was much higher than the global Ca^{2+} transient alone. The peak $(F/F_0)_d$ in an evoked nanotransient was 7.8-fold higher than that because of global Ca^{2+} elevation, providing direct evidence for a much higher cleft than global Ca^{2+} concentration in EC coupling (as expected from modeling studies).

Discussion

We have developed a novel Ca^{2+} imaging method that has enabled the first detection of Ca^{2+} signals arising in the submicroscopic (nanoscopic) space of the dyadic junction between the surface membrane and junctional SR. By analogy with Ca^{2+} sparks and to reflect the nanoscopic origin of the signal from our nondiffusible targeted probes, we introduce the neologism Ca^{2+} nanosparks to describe them. We show that targeted GCaMP6f-T/J provides a new and sensitive way of detecting dyadic activity, that is, when, where, and for how long a dyad is activated, even in cells undergoing vigorous contraction. Individual Ca^{2+} nanosparks are confined to a volume 50× smaller than conventional Ca^{2+} sparks as measured with diffusible indicators. Our approach is somewhat analogous to the use of GCaMP6f to count single neuronal synapse events.[16] However, we are dealing with a much smaller structure than a synaptic spine and, in this regard, it is remarkable that our nanoscopic signals had such good fidelity.

Imaging Ca^{2+} nanosparks has been made possible by the availability of a new generation of genetically encoded, ultrasensitive Ca^{2+} biosensor (GCaMP6f) and by the choice of proper targeting strategy. The fast kinetics, the high affinity, the high contrast factor of GCaMP6f collectively confers high sensitivity, whereas the fusion of biosensor to known dyadic proteins assures precise colocalization to the dyadic Ca^{2+}

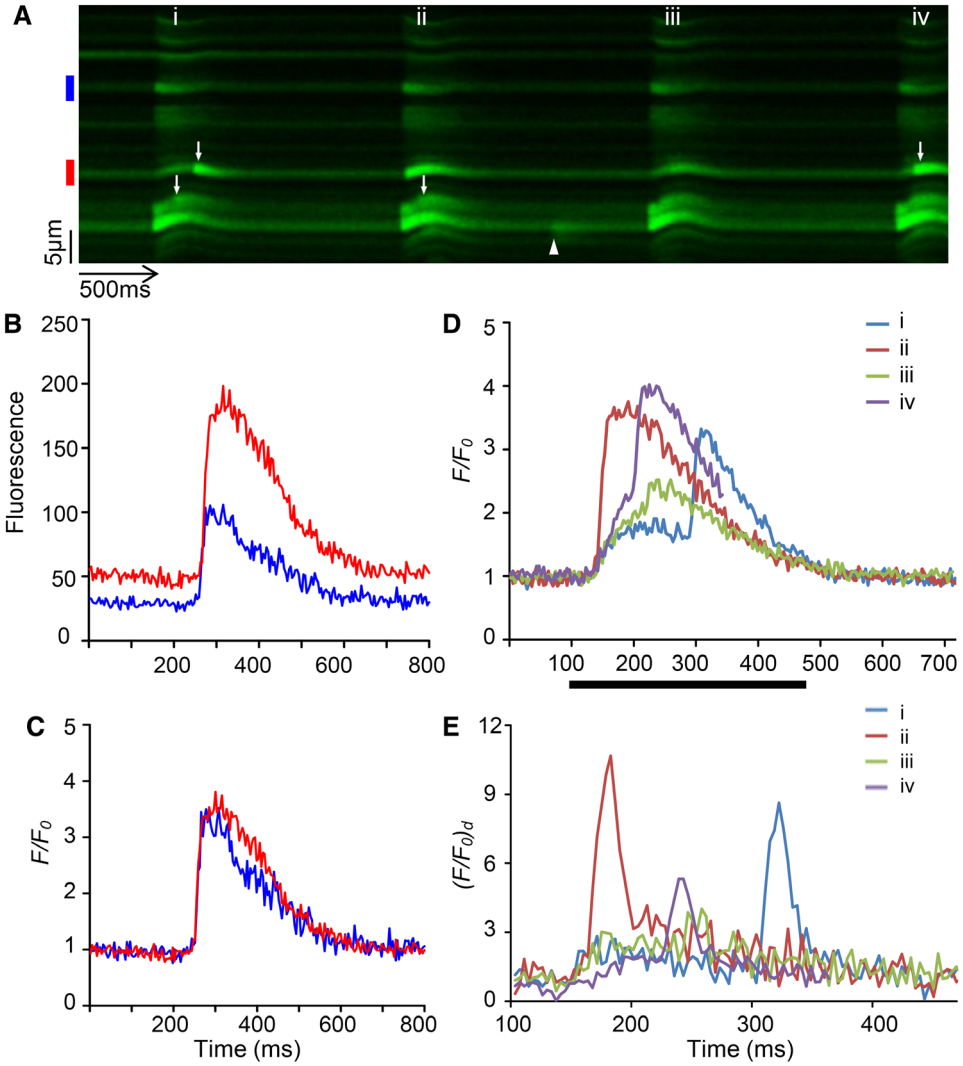

Figure 4. Dyadic Ca^{2+} signals in electrically paced cardiac myocytes. A, Evoked Ca^{2+} nanosparks in a cardiac myocyte under 1 Hz pacing. Arrows indicate late release events which can be clearly seen superimposed on the local Ca^{2+} changes. The distortion of the traces was because of cell contraction, showing normal excitation–contraction coupling was taking place. Solid arrowhead indicates a spontaneous nanospark. **B**, Time course of evoked signals. The time course of F/F_0 for the 2 regions is indicated in **A**, note the synchrony of the fluorescence changes although of differing brightness. This mainly reflects position of the confocal line scan relative to the dyad. **C**, Normalized (to prestimulus fluorescence) fluorescence has essentially the same amplitude during the Ca^{2+} transient. Therefore, the actual probe fluorescence change is not dependent on position relative to the confocal plane. **D**, Comparison of fluorescence changes during individual transients from a region (red) showing occasional late Ca^{2+} release events: (i and iv) Sudden rise of dyadic Ca^{2+} after a delay. ii, Synchronous activation of the dyad with others across the cell. iii, Dyad activation failure. **E**, as in **D**, for $(F/F_0)_d$ on an expanded time scale.

nanodomain. That the Ca^{2+} biosensor is immobile carries major advantages: not only does it permit a simple deconvolution to correct for the biosensor's turn-off kinetics, but also it obviates spatial blurring because of out-of-focus sampling that has confounded Ca^{2+} spark measurements. Serendipitously, we also found that the fusion of triadin/junctin to the C terminus of the biosensor also accelerated the turn-off rate of the biosensor, perhaps by facilitating the undocking of the M13–calmodulin complex. This suggests that further C-terminal modification might present a new strategy to further improve the kinetic properties of GCaMPs.

Although being highly sensitive, this new nanodomain Ca^{2+} measurement method also has a wide dynamic range. For example, it allows resolution of quarky Ca^{2+} release, spontaneous Ca^{2+} nanosparks, and even evoked Ca^{2+} nanosparks during the cell-wide Ca^{2+} transient. Analysis of the variability of Ca^{2+} nanospark amplitude provided new evidence that Ca^{2+} release is not necessarily all or none at the level of single dyads. Even at the same dyads, amplitudes of consecutive Ca^{2+} nanospark can vary ≈ 2-fold. These results imply stochastic recruitment of different numbers or subclusters of RyRs in a single functional dyadic junction. Our observation of some substructure within occasional Ca^{2+} nanosparks further supports the idea of possible subcluster activation within groups of RyRs[29] and previous reports of graded Ca^{2+} spark amplitude.[13,14] However, we have not yet observed temporally separable Ca^{2+} release events behavior within detectable subregions of single junctions, suggesting that RyR subclusters are spatiotemporally (and functionally) coupled within the ≈2 ms/0.3 μm resolution of the microscope. From this, we suggest that intrajunctional

activation propagation delays should be a minor component of the time to peak of the Ca^{2+} spark, consistent with Monte-Carlo simulations of the effect of RyR (re)organization on release time course within a single junctional region.[30]

By tracking individual dyad activation within the whole-cell contraction, the current work represents a substantial improvement over the previous Ca^{2+} spike method using heavy Ca^{2+} buffering.[12] It is especially important to note that the local biosensor did not disrupt normal EC coupling (as evidenced by a lack of effect on Ca^{2+} sparks). Therefore, although there may be some limited junctional buffering effect because of the sensor, cell-wide Ca^{2+} signals and Ca^{2+}-dependent regulation should be minimally perturbed.

Despite the biosensor's moderate K_d and the high Ca^{2+} concentration expected at the active dyads, we detected no sign of GCaMP6f-T/J saturation during a nanospark: the amplitude of nanosparks is smaller than that of nanotransients during action potential-elicited EC coupling and both were smaller than maximal GCaMP6f-T/J that could be obtained in steady-state calibrations. A possible explanation is that the relatively slow kinetics of the biosensor do not allow the biosensor to equilibrate during the saturating but short-lived dyadic cleft Ca^{2+} transient. Thus, a high-affinity, slowly responding probe may present relatively low-affinity behavior during highly dynamic Ca^{2+} signals. Furthermore, nonlinear interplay among multiple sensor Ca^{2+}-binding sites and temporal disparity between Ca^{2+}-binding and biosensor fluorescence may also contribute to this peculiar nonequilibrium property of the biosensor. These possibilities warrant future investigation and tuning of biosensor properties but are outside the scope of this article.

As a general problem that applies to all conventional fluorescent Ca^{2+} indicators, Ca^{2+} spark measurement with diffusible indicators grossly underestimates the local peak Ca^{2+} levels and reports a highly distorted spatial profile of local Ca^{2+} gradients.[31] Although the targeted sensors GCaMP6f-T/J can reveal Ca^{2+} release timing in the smallest domains (eg, a single dyad), we have not yet achieved the ambitious goal of directly reporting local Ca^{2+} levels within the junctional space, for reasons discussed above. Nevertheless, with the highly sensitive biosensor expressed at levels that did not significantly affect junction function, we obtained a Ca^{2+} signal (after temporal deblurring) that should provide an accurate measure of the local Ca^{2+} release duration and semiquantitative measurement of local Ca^{2+} fluxes.

Because heart failure and cardiac arrhythmias are often associated with dyssynchronous Ca^{2+} release, the ability of the probe to report release timing with good fidelity should facilitate investigation of the synchrony (or dyssynchrony) among release sites in health and diseases.[32,33] Our targeted Ca^{2+} biosensor approach may be extended to whole tissues and living organisms by transfection or transgenic techniques, and the lack of apparent effect of the biosensor on Ca^{2+} signaling suggests that it should not prevent normal Ca^{2+}-dependent signaling processes (eg, nuclear and cytoplasmic calmodulin signaling).

In summary, we have shown that high-quality intrajunctional Ca^{2+} release signals can be recorded as Ca^{2+} nanosparks with a novel targeted ultrasensitive biosensor. These Ca^{2+} nanosparks reveal junctional Ca^{2+} signaling in a way that is not possible with conventional diffusible Ca^{2+} indicators. Furthermore, this approach should be generally applicable to probing Ca^{2+} nanodomains (eg, clusters of inositol trisphosphate receptor Ca^{2+} release channels) in many cell types and even in living animals by transfection or transgenic approaches.

Acknowledgments

We thank Dr Looger from the Howard Hughes Medical Institute for the generous gift of GCaMP6 vectors and Dr Leslie M. Loew from University of Connecticut Health Center for Di-4 AN(F)PPTEA.

Sources of Funding

This work was supported by the National Key Basic Research Program of China (2011CB809100 and 2013CB531200), the National Science Foundation of China (31221002, 31130067, 31123004, 81370203, and 30900264), and the Royal Society UK.

Disclosures

None.

References

1. Franzini-Armstrong C, Protasi F, Ramesh V. Comparative ultrastructure of Ca^{2+} release units in skeletal and cardiac muscle. *Ann N Y Acad Sci*. 1998;853:20–30.
2. Grantham CJ, Cannell MB. Ca^{2+} influx during the cardiac action potential in guinea pig ventricular myocytes. *Circ Res*. 1996;79:194–200.
3. Allen DG, Blinks JR. Calcium transients in aequorin-injected frog cardiac muscle. *Nature*. 1978;273:509–513.
4. Wier WG. Calcium transients during excitation-contraction coupling in mammalian heart: aequorin signals of canine Purkinje fibers. *Science*. 1980;207:1085–1087.
5. Grynkiewicz G, Poenie M, Tsien RY. A new generation of Ca^{2+} indicators with greatly improved fluorescence properties. *J Biol Chem*. 1985;260:3440–3450.
6. Cannell MB, Berlin JR, Lederer WJ. Intracellular calcium in cardiac myocytes: calcium transients measured using fluorescence imaging. *Soc Gen Physiol Ser*. 1987;42:201–214.
7. Wier WG, Cannell MB, Berlin JR, Marban E, Lederer WJ. Cellular and subcellular heterogeneity of $[Ca^{2+}]_i$ in single heart cells revealed by fura-2. *Science*. 1987;235:325–328.
8. Cheng H, Lederer WJ, Cannell MB. Calcium sparks: elementary events underlying excitation-contraction coupling in heart muscle. *Science*. 1993;262:740–744.
9. Cheng H, Lederer WJ. Calcium sparks. *Physiol Rev*. 2008;88:1491–1545.
10. Stern MD. Theory of excitation-contraction coupling in cardiac muscle. *Biophys J*. 1992;63:497–517.
11. Wang SQ, Wei C, Zhao G, Brochet DX, Shen J, Song LS, Wang W, Yang D, Cheng H. Imaging microdomain Ca^{2+} in muscle cells. *Circ Res*. 2004;94:1011–1022.
12. Song LS, Sham JS, Stern MD, Lakatta EG, Cheng H. Direct measurement of SR release flux by tracking 'Ca^{2+} spikes' in rat cardiac myocytes. *J Physiol*. 1998;512(Pt 3):677–691.
13. Wang SQ, Song LS, Lakatta EG, Cheng H. Ca^{2+} signalling between single L-type Ca2+ channels and ryanodine receptors in heart cells. *Nature*. 2001;410:592–596.
14. Wang SQ, Stern MD, Ríos E, Cheng H. The quantal nature of Ca^{2+} sparks and in situ operation of the ryanodine receptor array in cardiac cells. *Proc Natl Acad Sci USA*. 2004;101:3979–3984.
15. Cannell MB, Kong CH. Local control in cardiac E-C coupling. *J Mol Cell Cardiol*. 2012;52:298–303.
16. Chen TW, Wardill TJ, Sun Y, Pulver SR, Renninger SL, Baohan A, Schreiter ER, Kerr RA, Orger MB, Jayaraman V, Looger LL, Svoboda K, Kim DS. Ultrasensitive fluorescent proteins for imaging neuronal activity. *Nature*. 2013;499:295–300.
17. Zhang L, Kelley J, Schmeisser G, Kobayashi YM, Jones LR. Complex formation between junctin, triadin, calsequestrin, and the ryanodine receptor. Proteins of the cardiac junctional sarcoplasmic reticulum membrane. *J Biol Chem*. 1997;272:23389–23397.
18. Huang X, Sun L, Ji S, Zhao T, Zhang W, Xu J, Zhang J, Wang Y, Wang X, Franzini-Armstrong C, Zheng M, Cheng H. Kissing and nanotunneling

mediate intermitochondrial communication in the heart. *Proc Natl Acad Sci USA*. 2013;110:2846–2851.
19. Yan P, Acker CD, Zhou WL, Lee P, Bollensdorff C, Negrean A, Lotti J, Sacconi L, Antic SD, Kohl P, Mansvelder HD, Pavone FS, Loew LM. Palette of fluorinated voltage-sensitive hemicyanine dyes. *Proc Natl Acad Sci USA*. 2012;109:20443–20448.
20. Soeller C, Crossman D, Gilbert R, Cannell MB. Analysis of ryanodine receptor clusters in rat and human cardiac myocytes. *Proc Natl Acad Sci USA*. 2007;104:14958–14963.
21. Nakai J, Ohkura M, Imoto K. A high signal-to-noise Ca^{2+} probe composed of a single green fluorescent protein. *Nat Biotechnol*. 2001;19:137–141.
22. Wang Q, Shui B, Kotlikoff MI, Sondermann H. Structural basis for calcium sensing by GCaMP2. *Structure*. 2008;16:1817–1827.
23. Hayashi T, Martone ME, Yu Z, Thor A, Doi M, Holst MJ, Ellisman MH, Hoshijima M. Three-dimensional electron microscopy reveals new details of membrane systems for Ca^{2+} signaling in the heart. *J Cell Sci*. 2009;122:1005–1013.
24. Laver DR, Kong CH, Imtiaz MS, Cannell MB. Termination of calcium-induced calcium release by induction decay: an emergent property of stochastic channel gating and molecular scale architecture. *J Mol Cell Cardiol*. 2013;54:98–100.
25. Soeller C, Cannell MB. Numerical simulation of local calcium movements during L-type calcium channel gating in the cardiac diad. *Biophys J*. 1997;73:97–111.
26. Kong CH, Laver DR, Cannell MB. Extraction of sub-microscopic Ca fluxes from blurred and noisy fluorescent indicator images with a detailed model fitting approach. *PLoS Comput Biol*. 2013;9:e1002931.
27. Brochet DX, Xie W, Yang D, Cheng H, Lederer WJ. Quarky calcium release in the heart. *Circ Res*. 2011;108:210–218.
28. Picht E, Zima AV, Shannon TR, Duncan AM, Blatter LA, Bers DM. Dynamic calcium movement inside cardiac sarcoplasmic reticulum during release. *Circ Res*. 2011;108:847–856.
29. Baddeley D, Jayasinghe ID, Lam L, Rossberger S, Cannell MB, Soeller C. Optical single-channel resolution imaging of the ryanodine receptor distribution in rat cardiac myocytes. *Proc Natl Acad Sci USA*. 2009;106:22275–22280.
30. Cannell MB, Kong CH, Imtiaz MS, Laver DR. Control of sarcoplasmic reticulum Ca^{2+} release by stochastic RyR gating within a 3D model of the cardiac dyad and importance of induction decay for CICR termination. *Biophys J*. 2013;104:2149–2159.
31. Smith GD, Keizer JE, Stern MD, Lederer WJ, Cheng H. A simple numerical model of calcium spark formation and detection in cardiac myocytes. *Biophys J*. 1998;75:15–32.
32. Litwin SE, Zhang D, Bridge JH. Dyssynchronous Ca^{2+} sparks in myocytes from infarcted hearts. *Circ Res*. 2000;87:1040–1047
33. Heinzel FR, MacQuaide N, Biesmans L, Sipido K. Dyssynchrony of Ca^{2+} release from the sarcoplasmic reticulum as subcellular mechanism of cardiac contractile dysfunction. *J Mol Cell Cardiol*. 2011;50:390–400.

Novelty and Significance

What Is Known?

- In cardiac dyads, junctional Ca^{2+} directly controls the gating of the ryanodine receptors (RyRs) and is itself dominated by RyR-mediated Ca^{2+} release from the sarcoplasmic reticulum.
- The stochastic timing of individual dyad Ca^{2+} release events that produce Ca^{2+} sparks governs the rising phase of the whole-cell Ca^{2+} transient.
- Conventional diffusible fluorescent Ca^{2+} indicators are unable to report Ca^{2+} in the dyadic junction, making it impossible to resolve individual dyad events during a fully activated Ca^{2+} transient.

What New Information Does This Article Contribute?

- A targeted, nondiffusible Ca^{2+} probe was developed by fusing the Ca^{2+} sensor GCaMP6f to the N terminus of triadin 1 and junctin, GCaMP6f-T/J, which resulted in its colocalization with RyRs.
- GCaMP6f-T/J reported Ca^{2+} nanosparks, which are Ca^{2+} signals associated with dyadic activation. Ca^{2+} nanosparks were spatially 50× smaller (by volume) than conventional Ca^{2+} sparks.
- Ca^{2+} nanosparks report when, where, and for how long an individual dyad is activated, even during the whole-cell Ca^{2+} transient and can reveal coactivation of subclusters of RyRs in the junction.

Ca^{2+} signaling is the result of nanoscopic Ca^{2+} kinetics in, for example, synapses and cardiac dyads. Imaging with diffusible Ca^{2+} indicators has, to date, visualized microscopic events such as Ca^{2+} sparks and Ca^{2+} puffs, which reflect the diffusion of Ca^{2+} from the sources but does not resolve the underlying nanoscopic Ca^{2+} kinetics. By fusing GCaMP6f (a new fast calmodulin-based fluorescent protein) to the N terminus of triadin 1 or junctin, which are known to traffic to dyads, we developed a nondiffusible Ca^{2+} probe, GCaMP6f-T/J. This probe colocalizes with RyRs and displays 4× faster off-kinetics than native GCaMP6f. This approach allowed the first detection of Ca^{2+} nanosparks at individual dyads, which are 50× smaller (by volume) than conventional Ca^{2+} sparks. Ca^{2+} nanosparks report when, where, and for how long a dyad is activated, even in cells undergoing vigorous contraction. In addition, we showed coactivation of subclusters of RyRs as well as all-or-none behavior in a single junctional region. This imaging strategy should be generally applicable to probing Ca^{2+} nanodomains in many cell types and even in living animals by transfection or transgenic approaches.

Ca^{2+} Nanosparks

Shining Light on the Dyadic Cleft But Missing the Intensity of Its Signal

Yan-Ting Zhao, Héctor H. Valdivia

Since the classical, many years ignored, and by current standards haphazard experiments of Sidney Ringer[1] on isolated rat hearts, we have come a long way in understanding the role of Ca^{2+} in the contraction of cardiac muscle. Ringer[1] found that suspending the hearts in a saline solution prepared with tap water (which contained high amounts of calcium carbonate from limestone) sustained robust contractions for a long time; but in an attempt to professionalize his art, Ringer[1] replaced tap water for distilled water, only to observe that in this clean medium, heart contractions declined quickly after only a few beats. By systematically adding different salts to the distilled saline medium, Ringer[1] discovered that calcium, until then considered exclusively a structural element of bones and teeth, was essential for cardiac muscle contraction. Since this serendipitous discovery, many others, in smaller or greater scale, kept adding to the inescapable notion that calcium ions (Ca^{2+}) play a critical role as a relay signal (a messenger) in many biological processes not only of cardiac myocytes, but also of virtually every living cell. Continuing with the story of Ca^{2+} in the heart, technically challenging experiments by Alexander Fabiato[2] defined, almost singlehandedly, the process of Ca^{2+}-induced Ca^{2+} release in cardiac cells, whereby a small amount of Ca^{2+} (in his case injected by a microsyringe on skinned cardiac tissue) caused a much larger release of Ca^{2+} from the sarcoplasmic reticulum (SR), inducing vigorous contractions. Fabiato's experiments, therefore, set the basis for a functional coupling between the sarcolemma (and its invaginations, the t-tubules) which injected Ca^{2+} by the voltage-induced opening of L-type Ca^{2+} channels (dihydropyridine receptors [DHPRs]) and the SR, which elicited massive Ca^{2+} release on binding of the incoming Ca^{2+} to ryanodine receptors (RyRs). Electron microscopy analysis of frozen skeletal and cardiac microsections, mainly the work of Franzini-Armstrong et al,[3] painstakingly reconstructed the structural arrangement of DHPRs and RyRs and helped define the microarchitecture of triads in skeletal muscle (SR–t-tubule–SR apposition) and dyads in cardiac muscle (SR separated from t-tubule by a tiny gap of ≈15–20 nm) in a mesoscopic scale. The concept of couplon was logically derived from these functional and structural interactions[4] and reaffirmed the association of voltage sensors in t-tubules (DHPRs) with Ca^{2+} release channels in the junctional SR (RyRs) in an inseparable functional unit. Thus, in an interesting saga from tap water to couplons (and many other intermediate steps omitted here for lack of space), the initial question of Ringer[1] (What ions are necessary for heart contractions?) has been refined to other questions such as those involving precise, nanoscale interactions between DHPRs and RyRs, the elusive Ca^{2+} gradient resulting from their almost simultaneous opening, the process quenching the regenerative nature of Ca^{2+}-induced Ca^{2+} release, the all-or-none versus graded recruitment of RyRs in a single dyad during normal e-c coupling, etc.

Article, see p 412

The sophistication of the current questions in e-c coupling would have not been possible without the recording of intracellular Ca^{2+} signals in cardiac cells. The first visualization of intracellular Ca^{2+} transients was reported by Allen and Blinks[5] in aequorin-injected frog cardiac muscle. The results were groundbreaking and revealed with fair approximation the cytosolic Ca^{2+} gradients achieved during single contractions for the first time. However, aequorin, a ≈22 kDa Ca^{2+}-sensitive chemiluminescent protein, is membrane impermeable and uses coelenterazine, which is irreversibly consumed to produce light, hence necessitating continuous addition of fresh protein into the media. These technical difficulties complicated the use of aequorin, and the widespread application of this technique never materialized. The arrival in 1985 of BAPTA-based Ca^{2+} indicators with capacity to permeate membranes, high Ca^{2+} affinity, and fast kinetics[6] made intracellular Ca^{2+} measurements the mainstay of many laboratories. Only 2 years after the introduction of Fura-2, Cannell et al[7] determined not only the magnitude of the Ca^{2+} transients in patch-clamped rat cardiomyocytes, but also their voltage-$[Ca^{2+}]_i$ relationship and the resting (diastolic) $[Ca^{2+}]$, establishing for the first time some of the most critical parameters of e-c coupling and revealing voltage ranges for maximal DHPR/RyR coupling efficiency. Finally, the introduction of fluorescein- and rhodamine-based Ca^{2+} indicators of high dynamic range and the advent of low-cost versatile confocal microscopes greatly facilitated the discovery of Ca^{2+} sparks, the localized, transient, and presumably elemental Ca^{2+} signaling events first detected in ventricular myocytes by Cheng et al.[8] Initially, Ca^{2+} sparks were thought to emanate from the opening of a single or a few RyR channels, but later studies pinpointed their origin to a cluster of RyRs, perhaps all those present in a single dyad. Although a single Ca^{2+} spark is an all-or-none or quantal event (but see below), recruitment of variable numbers of Ca^{2+} sparks allows for graded global Ca^{2+} release and hence contraction. Thus, the study of Ca^{2+} sparks provided direct evidence to the local control theory of e-c coupling[9] and helped resolve the conundrum pertaining to

From the Center for Arrhythmia Research and Division of Cardiovascular Medicine, Department of Internal Medicine, University of Michigan, Ann Arbor.

Correspondence to Héctor H. Valdivia, MD, PhD, Division of Cardiovascular Medicine, Department of Internal Medicine, University of Michigan, 2800 Plymouth Rd, 26-235N, Ann Arbor, MI 48109. E-mail hvaldiv@umich.edu

(*Circ Res*. 2014;114:396-398.)

***Circulation Research* is available at http://circres.ahajournals.org**
DOI: 10.1161/CIRCRESAHA.113.303112

the high-gain, regenerative nature of Ca^{2+}-induced Ca^{2+} release that predicted an all-or-none (instead of graded) Ca^{2+} release on cell depolarization. Fluo-3, the Ca^{2+} dye mostly used to detect Ca^{2+} sparks, displays fast Ca^{2+} association and dissociation kinetics (700 µmol/L per second and 369 per second, respectively) and could, in principle, return information on the Ca^{2+} dynamics of the dyadic cleft, but its fast diffusion coefficient distorts the spatial profile of the dyadic Ca^{2+} gradient, allows spatial blurring attributable to out-of-focus sampling, and precludes accurate estimation of the local peak Ca^{2+} level. Similarly, the use of intracellular solutions containing a fast, low-affinity Ca^{2+} indicator (such as Oregon Green 488 BAPTA 5N) and a slow, high-affinity Ca^{2+} buffer (EGTA) allows for detection of spatially restricted Ca^{2+} signals (Ca^{2+} spikes)[10] that approximate the waveform of Ca^{2+} release flux in a dyad but, because of the high (EGTA) and the diffusion of the Ca^{2+} indicator as mentioned above, this method also fails to return accurate information on the magnitude of the dyadic Ca^{2+} gradient.

In this issue of *Circulation Research*, Shang et al[11] made clever use of a nondiffusible, dyad-targeted Ca^{2+} biosensor to shed light, literally, on the Ca^{2+} dynamics that occur in the nanodomain of the dyadic cleft. The authors used GCaMP6f, a genetically encoded Ca^{2+} indicator composed of circularly permuted enhanced green fluorescent protein coupled to the Ca^{2+}-sensing protein calmodulin and to a calmodulin-binding peptide (the M13 fragment of myosin light chain kinase),[12] and fused it to the N-terminal of triadin (T) or junctin (J), 2 proteins that traffic to the junctional SR and apparently interact with the RyR. GCaMP6f is itself of bigger mass than triadin or junctin (≈32 and ≈26 kDa for the most common cardiac isoforms, respectively, see Figure) and is remarkable that junctin and triadin correctly target to the junctional SR despite such disproportionate cargo. Nevertheless, rat cardiac myocytes transfected with GCaMP6f-T/J display punctate fluorescence that partially overlaps with Di-4, an external membrane-bound dye and completely merges with RyR2 fluorescence, as expected if GCaMP6f-T/J was correctly trafficked to the junctional SR. In intact cells, the GCaMP6f-T/J fluorescence is spatially fixed, does not seem to interfere with normal Ca^{2+} signaling, and yields Ca^{2+} transients that are ≈50 times smaller in volume than customary Ca^{2+} sparks. Because these signals presumably arise from the nanodomain pertaining to a single dyadic cleft, the authors dubbed them Ca^{2+} nanosparks.[11]

It is pertinent to remark some attributes of GCaMP6f-T/J and its Ca^{2+} transient to appreciate fully what the term Ca^{2+} nanospark really defines. Because of the multiple steps involved in fluorescence generation on Ca^{2+} binding, GCaMPs display slow response kinetics (τ_{on}=20 ms–1.4 s)[15] compared with BAPTA-based indicators (τ_{on}=<1 ms). GCaMP6f is one of the fastest GCaMPs, and it was first used in neurons,[12] where it faithfully tracked single synapse events that occurred in the subsecond time scale. Here, Shang et al[11] found that GCaMP6f-T/J fusion to triadin increased its off rate ≈4-fold compared with native GCaMP6f, to 17 per second. Still, the on and off rates of GCaMP6f-T/J appear too slow for the rapidly rising and fast-decaying Ca^{2+} gradient that has been inferred by mathematical modeling for dyadic clefts of several animal species (see, for example, Cannell et al[14]). On injection of a few Ca^{2+} ions into the dyadic cleft by DHPRs, RyRs almost instantly open (τ_{on}≤1 ms),[16] generating Ca^{2+}-induced Ca^{2+} release and recruiting additional RyRs within the couplon. The merging of Ca^{2+} influx (I_{Ca}) and SR Ca^{2+} release generates local Ca^{2+} gradients that peak in ≈5 ms, persists for ≈15 ms, and reach levels upwards of 100 µmol/L.[14] In notorious disparity, calibration of GCaMP6f-T/J in situ yielded a Ca^{2+} dissociation constant (K_d) of 0.63 µmol/L, clearly too high an affinity for the peak Ca^{2+} gradient of the dyadic cleft. Thus, GCaMP6f-T/J, although correctly targeted and probably monitoring Ca^{2+} fluxes from the nanovicinity of RyRs, appears too slow and too avid for Ca^{2+} to report the fast Ca^{2+} gradient accurately that occurs in a typical dyadic cleft. As a consequence of its slow kinetics, GCaMP6f-T/J acts as a low-pass filter, severely attenuating the amplitude of the peak Ca^{2+} gradient (Figure). Therefore, the most defining features of these Ca^{2+} nanosparks are their reduced volume and their spatial immobility, but they should not be used to surmise on the magnitude of the dyadic Ca^{2+} gradient, one of the most elusive of the e-c coupling parameters of current times.

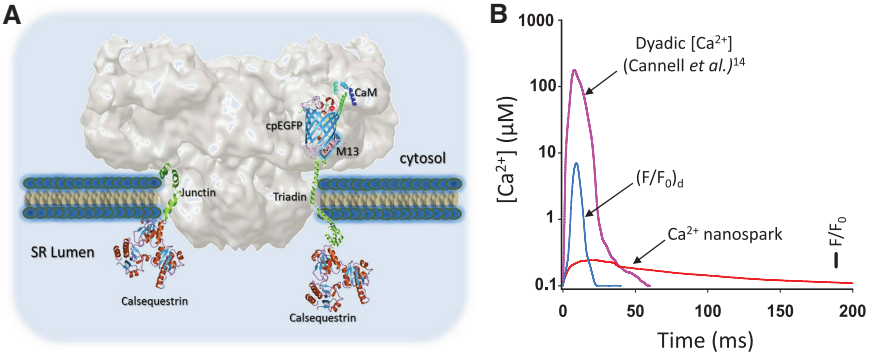

Figure. Ca^{2+} nanospark: molecules that detect it and its relationship to other dyadic Ca^{2+} parameters. **A**, Approximate 3-dimensional relationship between calmodulin (CaM)–circularly permuted enhanced green fluorescent protein (cpEGFP)–M13 peptide (GCaMP6f), triadin, and the ryanodine receptor (RyR). The faded gray structure is the cryo-electron microscopy surface representation of the RyR1 protein at 10 Å resolution (courtesy of M. Samsó). Triadin and junctin were generated by Song et al[13] using homology modeling. **B**, Estimated temporal relationship between the Ca^{2+} nanospark, the deconvolved Ca^{2+} nanospark signal $(F/F_0)_d$, and the estimated local Ca^{2+} gradient at the dyadic cleft (used with permission from Cannell et al[14]). Authorization for this adaptation has been obtained both from the owner of the copyright in the original work and from the owner of copyright in the translation or adaptation. See text for details. SR indicates sarcoplasmic reticulum.

How much farther will the Ca^{2+} nanosparks take the e-c coupling field? Are we witnessing a breakthrough of proportions akin to those of Allen and Blinks[5] and Cannell et al,[7] who introduced Ca^{2+} imaging to a field that had relied on electric signals to infer Ca^{2+} movements, or Cheng et al,[8] who ushered in an era of Ca^{2+} microdomains and took e-c coupling to the level of single couplons? Only time will tell. But even now, some advances are evident and need not wait for the verdict of time. By making straightforward assumptions on its on and off kinetics that allowed for deconvolution of its raw signal, Shang et al[11] obtained fair estimates of the Ca^{2+} fluxes that occur in the dyad, which are in turn a fair approximation of the RyR channels' open time. In essence, then, this new information is telling us for how long a dyad is activated, which had not been possible using diffusible Ca^{2+} indicators. Also, by virtue of the biosensor's spatial confinement, researchers will now be able to infer when and where a dyad is activated and, because GCaMP6f-T/J does not seem to interfere with normal Ca^{2+} signaling, these parameters may be obtained even in contracting cells. Perhaps more importantly, information derived from these signals is already challenging long-established dogmas of e-c coupling: if the Ca^{2+} nanosparks truly represent Ca^{2+} signals from single dyads, then different amplitudes (or substructures)[11] within a single Ca^{2+} nanospark may indeed represent different RyR clusters opening asynchronously (as postulated by the authors), which would not be expected from current local control models of couplon activation. Thus, there is uncontested merit in this novel approach. Although Ca^{2+} nanosparks do not report junctional Ca^{2+} levels with accuracy, neither do Ca^{2+} sparks report local cytoplasmic levels faithfully, yet, the latter have revolutionized our understanding of e-c coupling in fundamental ways.

Sources of Funding

H.H. Valdivia is a recipient of National Institutes of Health grants RO1-HL055438 and PO1 HL094291. Y.-T. Zhao has no grant support.

Disclosures

None.

References

1. Ringer S. A further contribution regarding the influence of the different constituents of the blood on the contraction of the heart. *J Physiol.* 1883;4:29–42.3
2. Fabiato A. Calcium-induced release of calcium from the cardiac sarcoplasmic reticulum. *Am J Physiol*. 1983;245:C1–C14.
3. Franzini-Armstrong C, Protasi F, Ramesh V. Comparative ultrastructure of Ca2+ release units in skeletal and cardiac muscle. *Ann NY Acad Sci*. 1998;853:20–30.
4. Stern MD, Pizarro G, Ríos E. Local control model of excitation-contraction coupling in skeletal muscle. *J Gen Physiol*. 1997;110:415–440.
5. Allen DG, Blinks JR. Calcium transients in aequorin-injected frog cardiac muscle. *Nature*. 1978;273:509–513.
6. Grynkiewicz G, Poenie M, Tsien RY. A new generation of Ca2+ indicators with greatly improved fluorescence properties. *J Biol Chem*. 1985;260:3440–3450.
7. Cannell MB, Berlin JR, Lederer WJ. Intracellular calcium in cardiac myocytes: calcium transients measured using fluorescence imaging. *Soc Gen Physiol Ser*. 1987;42:201–214.
8. Cheng H, Lederer WJ, Cannell MB. Calcium sparks: elementary events underlying excitation-contraction coupling in heart muscle. *Science*. 1993;262:740–744.
9. Stern MD. Theory of excitation-contraction coupling in cardiac muscle. *Biophys J*. 1992;63:497–517.
10. Song LS, Sham JS, Stern MD, Lakatta EG, Cheng H. Direct measurement of SR release flux by tracking 'Ca2+ spikes' in rat cardiac myocytes. *J Physiol.* 1998;512 (pt 3):677–691.
11. Shang W, Lu F, Sun T, Xu J, Li LL, Wang Y, Wang G, Chen L, Wang X, Cannell MB, Wang SQ, Cheng H. Imaging Ca2+ nanosparks in heart with a new targeted biosensor. *Circ Res*. 2014;114 412–420.
12. Chen TW, Wardill TJ, Sun Y, Pulver SR, Renninger SL, Baohan A, Schreiter ER, Kerr RA, Orger MB, Jayaraman V, Looger LL, Svoboda K, Kim DS. Ultrasensitive fluorescent proteins for imaging neuronal activity. *Nature*. 2013;499:295–300.
13. Song DW, Lee JG, Youn HS, Eom SH, Kim do H. Ryanodine receptor assembly: a novel systems biology approach to 3D mapping. *Prog Biophys Mol Biol*. 2011;105:145–161.
14. Cannell MB, Kong CH, Imtiaz MS, Laver DR. Control of sarcoplasmic reticulum Ca2+ release by stochastic RyR gating within a 3D model of the cardiac dyad and importance of induction decay for CICR termination. *Biophys J*. 2013;104:2149–2159.
15. Sun XR, Badura A, Pacheco DA, Lynch LA, Schneider ER, Taylor MP, Hogue IB, Enquist LW, Murthy M, Wang SS. Fast GCaMPs for improved tracking of neuronal activity. *Nat Commun.* 2013;4:2170.
16. Györke S, Fill M. Ryanodine receptor adaptation: control mechanism of Ca(2+)-induced Ca2+ release in heart. *Science*. 1993;260:807–809.

KEY WORDS: Editorials ■ calcium signaling ■ ryanodine receptor calcium release channel ■ sarcoplasmic reticulum